Tectonophysics 766 (2019) 326–339

Contents lists available at ScienceDirect

Tectonophysics

journal homepage: www.elsevier.com/locate/tecto

Kinematic and thermal evolution of the Haymana Basin, a fore-arc to foreland basin in Central Anatolia (Turkey)

Erhan Gülyüz[a,*], Murat Özkaptan[b], Nuretdin Kaymakci[c], Cristina Persano[d], Finlay M. Stuart[e]

[a] Department of Geological Engineering, Yüzüncü Yıl University, Van, Turkey
[b] Department of Geophysical Engineering, Karadeniz Technical University, Trabzon, Turkey
[c] Department of Geological Engineering, Middle East Technical University, Ankara, Turkey
[d] School of Geographical and Earth Sciences, University of Glasgow, Glasgow, Scotland, United Kingdom of Great Britain and Northern Ireland
[e] Isotope Geosciences Unit, Scottish Universities Environmental Research Centre, East Kilbride, Scotland, United Kingdom of Great Britain and Northern Ireland

ARTICLE INFO

Keywords:
Haymana Basin
Central Anatolia
Foreland
Forearc
Apatite-Helium

ABSTRACT

Gondwana (Tauride/Kırşehir blocks) and Eurasia (Pontides) derived continental blocks delimit the Haymana basin, central Turkey, to the south and the north, respectively. The boundaries of these blocks define the Izmir-Ankara-Erzincan and Intra-Tauride Suture zones which are straddled by a number of Late Cretaceous to Oligocene marine to continental basins. The Haymana Basin is located at the junction of the IAESZ and ITSZ and comprises Upper Cretaceous to Middle Eocene basin infill deposited in response to the interaction of these blocks. The basin provides a unique opportunity to unravel spatio-temporal relationships related to the timing of late stage subduction history of Neo-Tethys Ocean and subsequent collision of the intervening continental blocks. We have conducted a multidisciplinary study in the region that includes mapping of major structures combined with fault kinematic analyses. E-W striking folds dominate the basin, cross-section balancing of these structures indicates around 25% roughly N-S shortening in the region. Paleostress studies indicate that the basin was initially subjected to N-S to NNE-SSW extension until the middle Paleocene (phase 1) and then N-S directed *syn*-depositional compression and coeval E-W directed extension until the middle Miocene (phase 2) implying strike-slip deformation and pure shear shortening in the basin. These different deformation phases are attributed to first fore-arc (subduction) basin development then foreland (collision) stages of the basin. Apatite (U-Th)/He dating of 5 samples indicate that exhumation of the SE segment of the basin started in early Oligocene, whereas the NW segment of the basin exhumed in the early Miocene. The differential uplift is possibly related to progressive north-westwards movement of Dereköy basin bounding fault at the north. We propose that the Haymana basin evolved from extensional forearc basin during the late Cretaceous to early Paleocene and foreland basin after the terminal subduction and subsequent collision of Tauride and Pontide blocks.

1. Introduction

Sedimentary basins are key areas in understanding both opening and closure histories of ancient oceans and subsequent collision histories of continental margins since they record these events in their infill. In order to unravel the coupling between basin evolution and evolution history of related oceanic domain, basically; understanding the geometry, tectonic setting, stratigraphy, structural and tectonic characteristics and their spatio-temporal evolution are crucial.

The Late Cretaceous to Paleogene evolution of Anatolia is dominated by development of an array of fore-arc to foreland basins (Fig. 1A & B) owing to terminal northwards subduction and obliteration of the Neotethys Ocean (Fig. 1A & B) that gave way to the development of Izmir-Ankara-Erzincan Suture zone. Opening of the Neotethys Ocean took place between Laurasia in the north and Gondwana in the south, during early Mesozoic in two branches in Turkey (Şengor and Yilmaz, 1981). The northern branch separated the Pontides, a landmass with Laurasian affinity and Hercynian basement in the north, the Taurides comprising metamorphosed zones along its northern margin (e.g. Tavşanlı and Afyon zones) and, the Kırşehir Block, in the south (Şengor and Yilmaz, 1981; Okay, 1984; Okay and Tüysüz, 1999). The Taurides was a passive margin during the evolution of the Neotehys and are characterized mainly by Paleozoic to Mesozoic carbonate platform while the Pontides were converted into an active margin possibly

* Corresponding author.
E-mail addresses: erhangulyuz@yyu.edu.tr (E. Gülyüz), kaymakci@metu.edu.tr (N. Kaymakci), Cristina.Persano@glasgow.ac.uk (C. Persano), Fin.Stuart@glasgow.ac.uk (F.M. Stuart).

https://doi.org/10.1016/j.tecto.2019.06.020
Received 31 January 2019; Received in revised form 14 June 2019; Accepted 23 June 2019
Available online 27 June 2019
0040-1951/

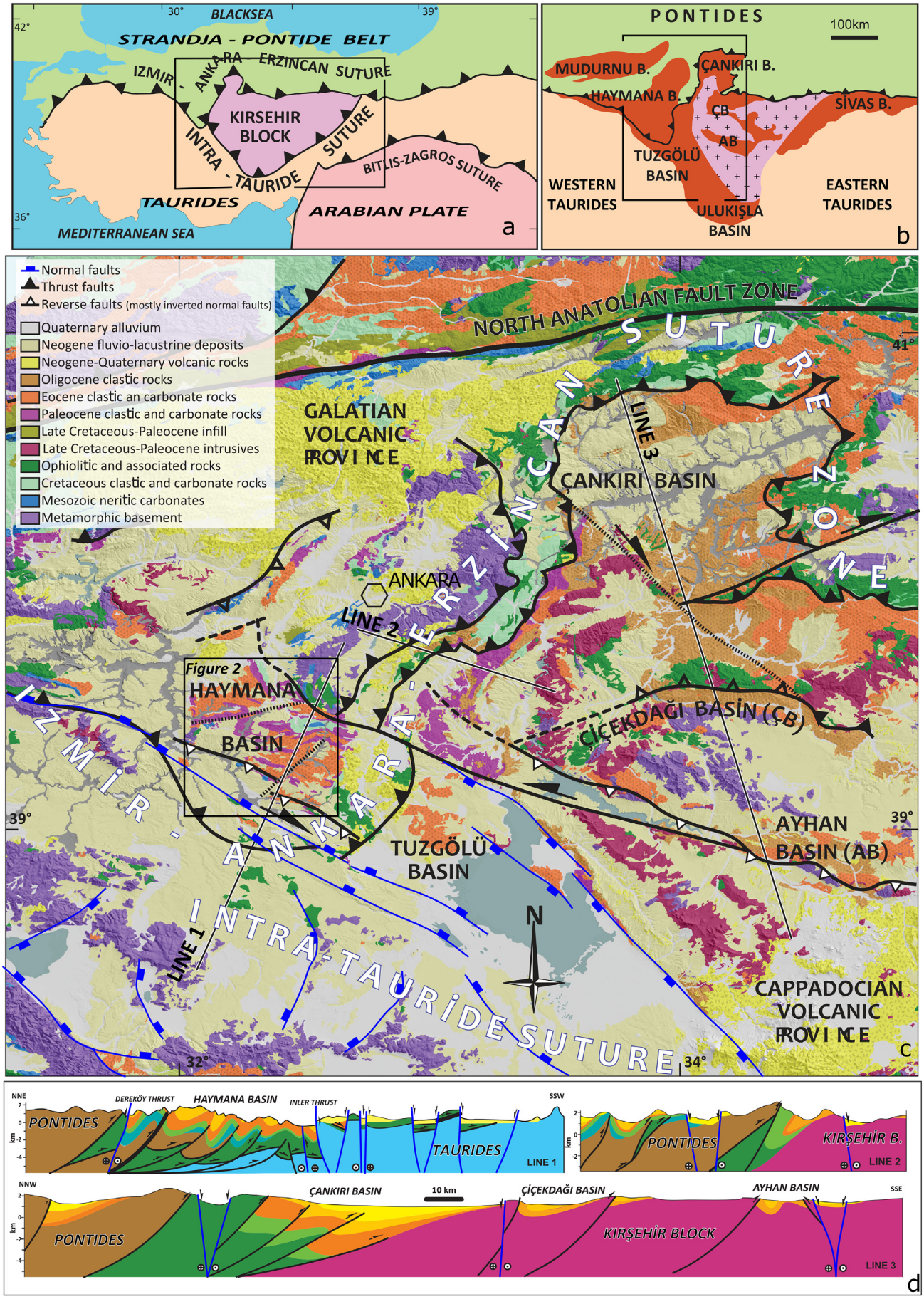

(caption on next page)

Fig. 1. Geological setting of the Haymana Basin. (A) Major tectonic divisions of Anatolia (modified Görür et al., 1984); (B) Mesozoic and Cenozoic basins in central and northern Anatolia, (modified Görür et al., 1984, Özsayın and Dirik, 2007; Kaymakci, 2000; Kaymakci et al., 2009). (C) Geological map of the Central Anatolia (modified from MTA 2002 map); (D) Crustal scale cross-sections showing association of the basins and tectonic blocks of the Central Anatolia. Circle shows the location of the study area and blue lines in C shows the cross-section lines in D.

during the early Cretaceous after the inception of northwards subduction below the Pontide continent (Şengor and Yilmaz, 1981; Okay and Tüysüz, 1999; Kaymakci et al., 2009). This is evidenced by (i) disruption of Late Jurassic to Early Cretaceous carbonate platform and development of small isolated basin complexes in which widespread continental to marine clastic deposition took place from the Barremian onwards (Hippolyte et al., 2010, 2018) and (ii) Late Cretaceous to Eocene arc-related magmatic products on the Pontides (Toprak et al., 1996; Keskin et al., 2008; Arslan et al., 2013; Speciale et al., 2014). Deposition and subsequent magmatism and metamorphism took place during much of late Cretaceous. In the meantime an array of fore-arc basin complexes that developed at the southern margin of the Pontides were established (Koçyiğit, 1991; Kaymakci et al., 2009; Okay et al., 2019). By the end of Cretaceous, due to terminal subduction and obliteration of the Neotethys in Turkey, these basins were partly destroyed and incorporated into an imbricate thrust belt along the Izmir-Ankara-Erzincan Suture Zone (IAESZ), which accreted and intensely deformed during the collision and further convergence of the tectonic blocks involved.

Two scenarios have been suggested for the timing and evolution of the Neotethys in Central Anatolia. Görür et al. (1984, 1998) and Rice et al. (2006), based on relatively dated deformation phases determined in Tuzgölü and Sivas basins, claim that collision and suturing along the Izmir-Ankara Erzincan Suture took place during the Eocene, although termination of ophiolitic mélange formation and first docking of Pontides and Taurides took place during the latest Cretaceous (Okay et al., 2013). However, Tüysüz et al. (1995), Okay and Tüysüz (1999), Kaymakci et al. (2009) and Gülyüz et al. (2013), mainly based on tracing deformation events on both sedimentary basins and metamorphic rocks argue that Tauride and Kırşehir blocks are progressively collided and amalgamated along the İzmir-Ankara-Erzincan (IAESZ) in the north and Intra-Tauride suture zones (ITSZ) (Fig. 1a) in the south. In this model the latest subduction and accretion process along the IAESZ and related development of fore-arc basins lasted until the end of Cretaceous. Paleocene to Oligocene time interval in the region is dominated by foreland deposition along the southern margin of Pontides within the Haymana, Çankırı and Sivas basins (Kaymakci, 2000; Kaymakci et al., 2009; Rice et al., 2006; Gülyüz et al., 2013; Legeay et al., 2018; Darin et al., 2018) while the underlying Gondwana derived blocks experienced coeval burial and metamorphism. Peak metamorphic ages correspond to Campanian (late Cretaceous) to Paleocene time interval (Pourteau et al., 2010, 2013, 2016, 2019). Exhumation of the Kırşehir Block in extensional settings by the end of Cretaceous (Lefebvre, 2011 and Lefebvre et al., 2015) gave way to the development of supra detachment basins such as the Late Cretaceous – Oligocene Ayhan Basin (Advokaat et al., 2014). Apart from the basin on the Kırşehir Block several basins were developed within the Pontides, Kırşehir Block and Tauride-Anatolide Block (Fig. 1B & C), among these the Çankırı, Sivas and Haymana basins (Kaymakci et al., 2009) were evolved from fore-arc basins during the late Cretaceous into foreland basins during the Paleocene. However, the Tuzgölü, Ulukışla, Ayhan and Çiçekdağ basins straddle the Tauride and Kırşehir blocks and developed during the latest Cetaceous to Paleogene during the collision and further convergence of Pontides and the Taurides.

Among the Central Anatolian basins, the Haymana basin has a key location where İAESZ and the debatable ITSZ coincide (Fig. 1B). In addition, the basin provides an ideal opportunity to understand changes in deformation styles and depositional setting throughout the complete closure of an ancient ocean since it comprises late Cretaceous-Paleogene sequences which temporally covers late stage subduction of the Neotethys Ocean and collision between continental blocks. However, the Haymana basin is poorly defined in terms of style of deformation, tectonic evolution and basin type while other Central Anatolian basins (e.g. Sivas, Çankırı, Tuzgölü, Ayhan, Çiçekdağı, Ulukışla, Hekimhan basins) are well documented in terms of their tectono-stratigraphic evolution (Kaymakci, 2000; Rice et al., 2006; Kaymakci et al., 2009; Çemen et al., 1999; Nairn et al., 2013; Clark and Robertson, 2002; Advokaat et al., 2014; Gülyüz et al., 2013). In this regard, the main of this study is to unravel the structural and low temperature thermal evolution of the Haymana basin by focusing on by field observations, fault kinematics, cross-section balancing and low-temperature thermochronologically.

This study has revealed significant new evidence for (i) timing of continental collision between Tauride and Pontide blocks in the central segment of the IAESZ, and (ii) changes in deformation styles throughout the progressive convergence of intervening continental blocks. The study emphasizes the importance of understanding structures and thermal history of a foreland basin for unraveling deformation history of a region.

2. Geological background

2.1. Stratigraphic development of the Haymana Basin

The Haymana Basin contains approximately 8 km of sedimentary sequences (Ünalan et al., 1976) comprising four distinct vertically and laterally gradational cycles from late Cretaceous to late Eocene (Fig. 2A & B) (Gülyüz, 2015). These are unconformably overlain by the Neogene continental sequences which cover larger areas and not constrained to the present boundaries of the basin (Fig. 2B).

In contrast to the complex structure of the basement units, ~8 km-thick infill of the Haymana basin comprises four vertically gradational well-developed depositional cycles from Late Cretaceous to Late Eocene covered by Neogene continental units (Fig. 2A–B) (Gülyüz, 2015). The main definition criteria for the depositional cycles are the depositional environment of the basin infill and their lateral/vertical stratigraphic continuity (time-dependent) and each cycle is defined as a group, including continental clastic rocks, shallow- and deep-marine deposits. The first cycle comprises upper Cretaceous Haymana and Beyobası formations (Sirel, 1975; Ünalan et al., 1976; Toker, 1979) belonging to its fore-arc basin configuration. The proximal equivalents of the cycles are defined as İncirli formation in the Orhaniye Basin which is located out of the mapped area (Koçyiğit, 1991). The Haymana Formation includes mainly turbidites and fine clastics intercalated with occasional marls, whereas the Beyobası Formation is characterized by shallow-marine carbonates and clastics intercalated with coal horizons. A sedimentological study conducted on the sandstone layers of the Haymana Formation (Çetin et al., 1986) indicates that (i) mainly acidic intrusions related grains together with the ophiolitic/metamorphic fragments are the basic population of the sandstone layers. According to Çetin et al. (1986) the sandstone grains indicates intra- or fore-arc environment for the deposition of the unit. Also, *syn*-sedimentary primary features indicating N-NW to S-SE sediment transport directions (Çetin et al., 1986) are frequently observed. The first cycle grades into the lower Paleocene (Sirel et al., 1986) second cycle which comprises Paleocene Kartal, Çaldağ and Yeşilyurt formations. The Kartal Formation comprises continental red clastic rocks and is developed extensively as the proximal facies in most of the Central Anatolian basins. It overlies the first cycle rocks with local unconformity while the other relatively distal facies of the second cycle are conformable with the first

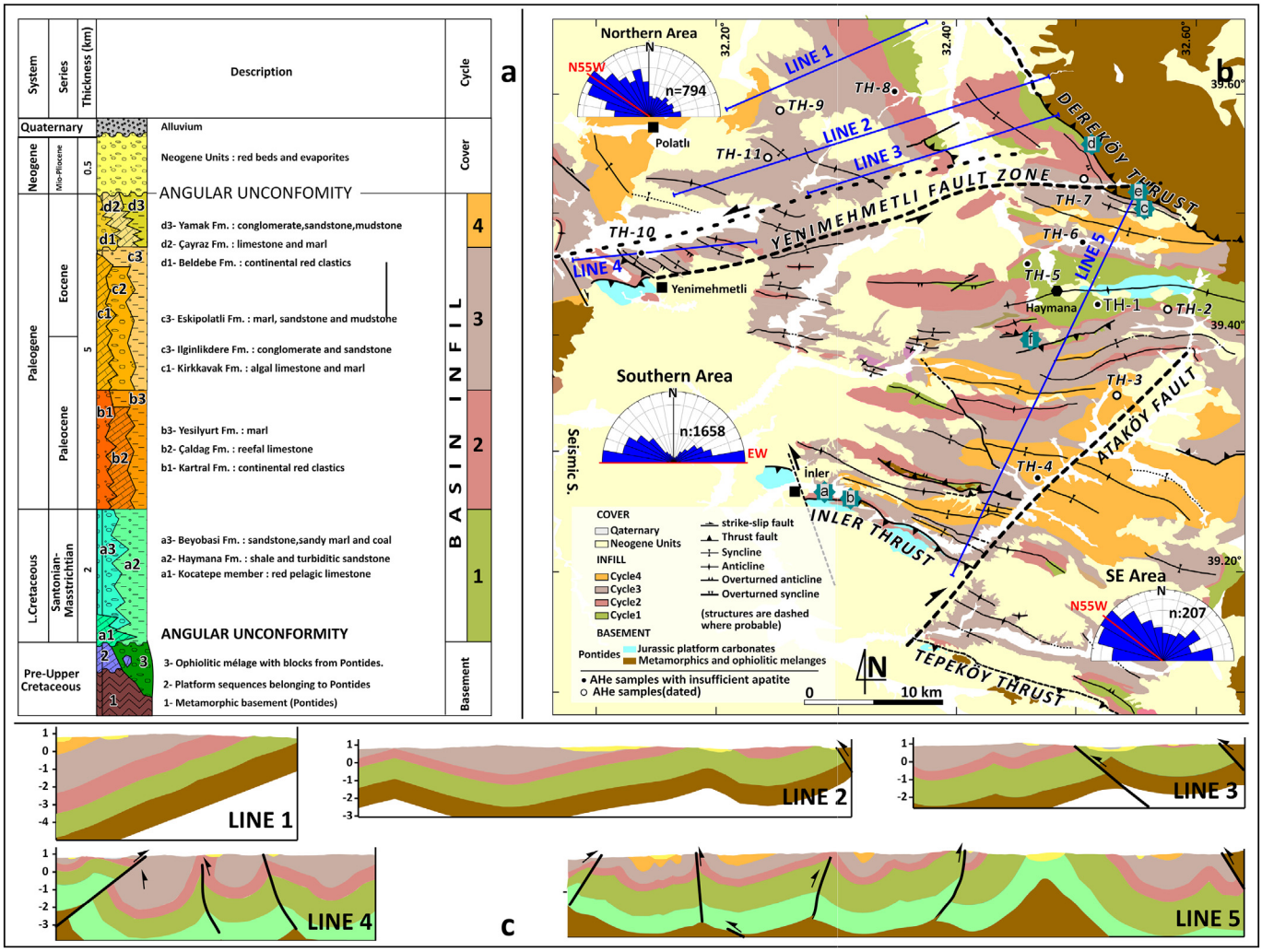

Fig. 2. (A) Columnar stratigraphic section of the Haymana basin (modified after Ünalan et al., 1976), (B) Geological map of the Haymana basin, C) Balanced Cross-sections. Academic version of Midland Valley Move 2015.1 software was used to construct the sections. Based on 1B fold classes (parallel folding) of Ramsay (1967) allowing to take constant bed height and more accurately model post-depositional deformation occurred in the basins (Dahlstrom, 1969), the folds were constructed for the deformed state. Note: TH symbols with numbers in A represent the stratigraphic positions of the dated Apatite-He samples, rose diagrams represent the main strike trends measured in different segments of the basin, labeled blue stars show the locations of pictures given in Fig. 4.

cycle. Kartal Formation laterally grades into Çaldağ and Yeşilyurt formations. The Çaldağ Formation is characterized by neritic facies dominated by reef limestones and the Yeşilyurt Formation consists of deeper marine turbidites. The third cycle in the basin comprises the upper Paleocene to lower Eocene (Ünalan et al., 1976) Kırkkavak, Eskipolatlı and Ilgınlıkdere formations. The Kırkkavak Formation is composed of shallow-marine deposits associated with continental clastics, whereas the Ilgınlıkdere and Eskipolatlı formations are characterized by slope and slope front deeper marine clastics with frequently observed slumps (Gülyüz, 2015), respectively. The fourth cycle comprises the Lower to middle Eocene (Sirel, 1976; Gülyüz, 2015) Beldede, Çayraz and Yamak formations. The Beldede Formation is represented by continental red clastics while Çayraz and Yamak formations are deposited in a shallow-marine to deeper-marine environments respectively.

The boundary relationships between these units and the cycles are complex. Although there are conformable vertical gradations in the distal sequences, the marginal sequences have progressive unconformities (cf. Riba, 1976). The origin of these unconformities may be due to the coupling between tectonic deformation and deposition, since they have angular relationships in places unlike disconformities which would been developed in the case of sea level fluctuations which is not the case here.

Another peculiar relationship in the basin infill is related to consistent coarsening and thickening upward relationships between the cycles in contrast to the within-cycle fining upward relationships. This is interpreted as basin filling that is possibly coupled with sea level fluctuations and tectonics. Abrupt shallowing from deep marine conditions to shallow marine conditions is also noted within the cycles. This is attributed to differential uplift and major sea level drops during the evolution of the basin (Gülyüz, 2015).

2.2. Thermal history constraints

Low-temperature thermochronology studies in the region are limited only on the exhumation histories of the crystalline basement rocks; the western Pontides (Cavazza et al., 2012), the eastern Pontides (Boztuğ et al., 2004), and the Kırsehir Block (Whitney et al., 2001, 2008; Fayon et al., 2001; Boztuğ and Jonckheere, 2007). Cavazza et al. (2012) argued that three discrete phases of exhumation took place in the western Pontides, although their data suggest a continuous spectrum of uplift and exhumation where no clear break between these discrete events could be separated. They ascribed the first phase to the terminal closure of the Neo-Tethys Ocean and the onset of the collision

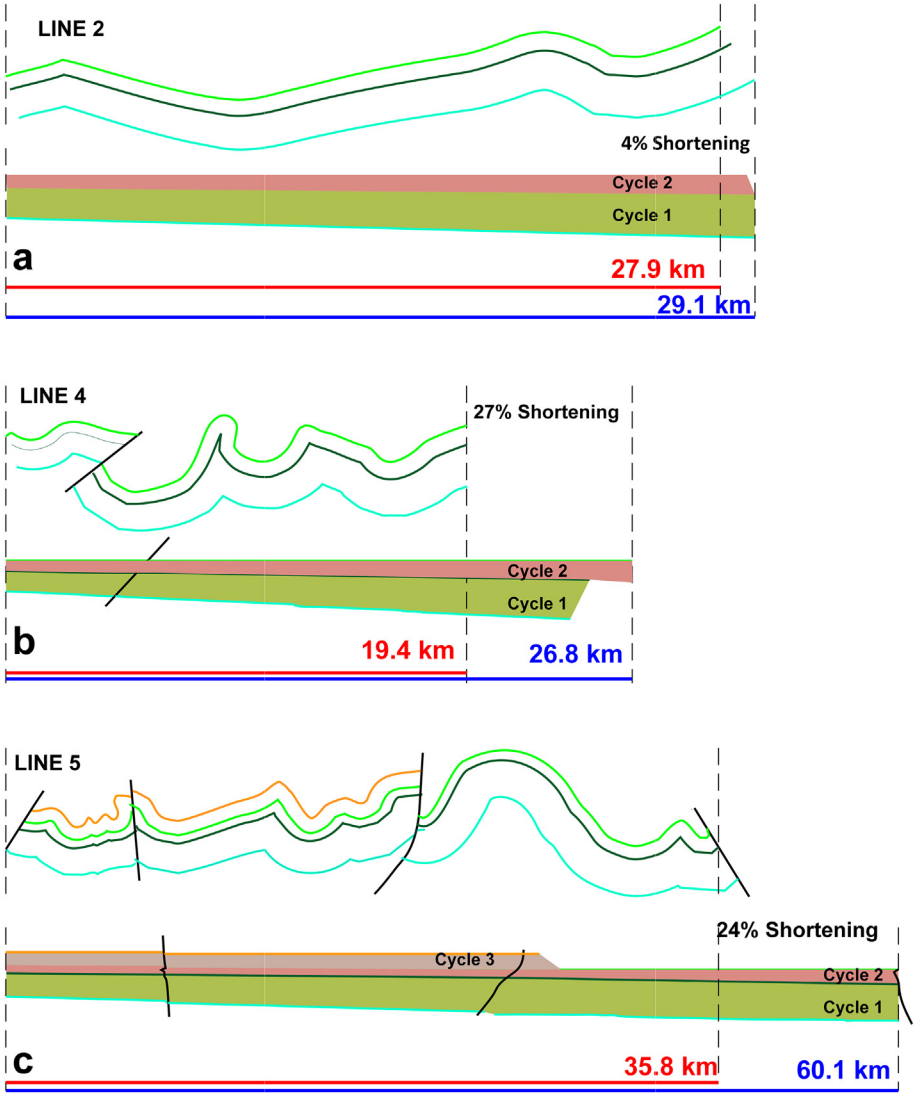

Fig. 3. Shortening ratio calculations. Note that blue lines indicate initial (expected) length of the horizons and the red lines indicate the length of deformed horizons. See Fig. 2 B for the traces of the cross-sections.

of Pontides and the Tauride and Kırşehir blocks by the end of Cretaceous. The second phase was ascribed to a renewed tectonic activity along the IAESZ. They related the last phase to the onset of Aegean extension.

Boztuğ et al. (2004) defined three different cooling events without clear boundaries corresponding to the three distinct exhumation events along the eastern Pontides. The first phase, late Cretaceous to late Paleocene, is attributed to the closure of the Neo-Tethys Ocean along the easternmost segment of the IAESZ while late Paleocene-early Eocene phase is attributed to the closure of the ocean along the relatively western segment and the third phase that cover the Miocene-Pliocene time interval is attributed to the collision of Arabian Plate along the Bitlis Suture Zone and subsequent inception of the North Anatolian Fault Zone. Boztuğ and Jonckheere (2007) suggested that Paleocene-Eocene exhumation ages from the northern margin of the Kırşehir Block record the collision and related regional uplift in the region. Whitney et al. (2001, 2008) and Fayon et al. (2001) agree with the Boztuğ and Jonckheere (2007) for the northern margin of the block, however, they also argued that Oligocene-Miocene cooling ages of the southern margin are related to the escape tectonics related to westwards escape of Anatolian Block along the North and East Anatolian fault zones. However, Gautier et al. (2002, 2008) relate these young ages to reheating and thermal resetting due to widespread Cappadocian and coeval magmatism in the region. All these studies give limited exhumation ages from only crystalline rocks without any local kinematic data. Therefore tectonic interpretations relating the exhumation ages with the collision along the Neo-Tethyan suture zones are open to discussion.

3. Results

3.1. Structural analyses of the Haymana Basin

Main structures shaping the present geometry and responsible for the inversion of the basin are approximately E-W striking folds and two basin bounding faults namely Dereköy, İnler and Tepeköy thrusts. Yenimehmetli Fault Zone (YFZ) divides the basin into two sectors as Northern and Southern sectors based on dominant trends of the folds (Fig. 2B).

3.1.1. Folds

The present scheme of the basin is dominated by folds into which most of the basin infill are exposed. In the northern and southern part of the Haymana Basin Jurassic to Cretaceous basement rocks belonging to the Pontides are exposed (Fig. 2B), while in the south the rocks belonging to the Taurides are exposed just outside of our mapped area.

Additionally, the contact between the Tauride and basin infill is covered by Neogene deposits (Fig. 1C). In large part of the basin, the Jurassic-Cretaceous rocks constitute the basement and they are involved in the deformation and structural development of the basin infill. To understand the structural characteristics and evolution of these structures, > 2800 bedding attitudes were collected from the infill (supplements). Based on these data 46 major folds are mapped out and are indicated with universal fold symbols in Fig. 2B. These data, together with field observations are used to construct five balanced cross-sections which are restored and used to quantify shortening amounts and ratios in the basin.

Results indicate that the bedding strikes dominate into two main directions; N55 W in the northern and SE part of the basin while in the central part of the basin the mode of the strikes is about EW (Fig. 2B). Dip amounts change between 30° to 50° chiefly. Similarly, 17 of the 46 folds mapped out in the basin are trending approximately E-W directions mainly in the central and SE part of the study area while remaining 29 of them are oriented NW-SE in the northern areas. Folds in the northern and southern margins of the basin have 70°–80° dipping axial planes whereas folds in the center of the basin have sub-vertical axial planes.

For the restoration of the cross-sections, flexural-slip unfolding method which is the most proper method for restoring sedimentary folds is used. In this method, the area of the stratigraphic cycles and line length of the youngest basin infill units are preserved (c.f. Dahlstrom, 1969). In other words, it is assumed that layer-parallel slip took place during folding and the amount of slip increases away from hinge lines of the folds towards the inflection lines on the limbs similar to logic of 1B fold (parallel folding, Ramsay, 1967) formation mechanism. Therefore, during restoration the horizons are rotated to the horizontal by removing the flexural slip components of the folds. This procedure allows us to get the most reliable shortening calculations for the sedimentary basins in which 1B class folds are expected to develop. After unfolding procedure completed, the attitude of the fault planes and offset amounts were adjusted accordingly.

The results of the balanced sections and shortening ratio calculations indicated that shortening amounts are not equal in the northern and southern sectors of the basin (Fig. 3). The northern areas of the basin are least deformed with an average shortening ratio of 3% while the total true thickness of the basin infill reaches up to 6 km. Complexity and deformation amounts are higher in the southern parts with an average 24% shortening ratio. However, the largest shortening is obtained parallel to the Yenimehmetli Fault Zone (Figs. 2B & 3).

In the core of the Haymana Anticline (around Th-1 and Th-2, in Fig. 2A & B) the Jurassic-Cretaceous carbonate units belonging to the Pontide basement are exposed. Therefore in this anticline maximum amount of erosion took place and it is calculated to be around and > 5 km.

3.1.2. Faults

The major faults controlling the deformation in the Haymana basin are the basin bounding faults in the northern and southern margin of the basin and two major strike-slip faults that compartmentalize the basin into domains of different deformation intensity and direction.

The Dereköy Thrust delimits the northern boundary of the basin developed between basement rocks and the basin infill while İnler and Tepeköy thrust faults delimits the basin from the south (Fig. 4A–D). Along the Dereköy Thrust basement rocks belonging to the Pontides thrust over the basin infill units and it is sealed by Neogene units. In the south, similarly along the İnler and Tepeköy thrusts the Pontide basement rocks thrust over the basin infill.

Along the Ataköy Fault, it seems that the İnler and Tepeköy thrusts are displaced dextrally and possibly they were parts of the same thrust fault before. Also, several small-scale strike-slip faults with WSW–ENE, E–W and NW–SE strikes are also encountered in the basin (Figs. 2B & 4F).

3.1.3. Paleostress analyses

Determining the principal stress orientations of an individual deformation phase is the main aim of the paleostress analyses. Various methods have been suggested for this inverse solution (e.g. Angelier, 1979, 1984, 1994; Armijo et al., 1982; Hardcastle, 1989; Shan et al., 2003) and they all assume that (i) analyzed rock volume (physically/mechanically homogeneous and isotropic) rheologically acts as linear material, (ii) ductile deformation within the rock volume and rotation on fault planes do not occur, (iii) the rock volume is deformed under a spatio-temporally unchanged stress regime, and (iv) the direction of resolved maximum shear stress is parallel to direction of movement vector on the fault plane, and the movement along a fault is independent of the other faults under the same tectonic regime. In addition to these assumptions, data acquisition from fault planes, and separation of deformation phases found in same data cloud (same region) are the major bias factors that must be taken into account for reliable paleostress analyses (Sperner and Zweigel, 2010). Despite these biases and weaknesses of different stress inversion methods and variation in the scale and tectonic meaning of the results of contemporary stress and paleostress measurements, Lacombe (2012) demonstrated the reliability of inversion procedures to understand contemporary and ancient stress behaviors of long-lived geological processes such as continental collisions.

The stress inversion procedure developed by Angelier (1979) relies on nine parameters, three of them are related to the orientation of the slip vector on each fault plane and is measured in the field, three of them are the orientations, and the remaining three are the magnitudes of the principal stresses. Since the absolute paleostress magnitudes cannot be determined only by using the fault slip data sets, Angelier (1979) proposed the reduced stress tensor concept, which decreased the six unknown parameters down to four by using the shape factor of the paleostress ellipsoid ($\Phi = (\sigma2-\sigma3)/(\sigma1-\sigma3)$). The shape factor is determined by the relative magnitudes of the principal stresses. Therefore, the paleostress orientations can be determined by at least four fault slip data to be collected in the field and are assumed to be the resolved shear stress (Wallace 1953 and Bott 1959) on the fault plane for the same stress regime. Then the type of the stress regime is deduced based on Anderson (1951). In other words, near vertical, if not vertical, σ1 indicates extensional, s2 strike-slip, and σthree thrusting (contractional) stress regime. All other cases imply a combination of these regimes. Care must be given, in the case of interpretations of the paleotress orientations, on the fact that local variations and stress permutations may lead to incorrect conclusions. Especially, in strike-slip regimes, local stress variations are very common depending on the change in the fault trace and step-overs. Same is true at fault terminations and transfer zones in normal and reverse faults (Hartz and Andresen, 1997; Homberg et al., 2002; Hu and Angelier, 2004; Lacombe et al., 2006; Pollard et al., 1993; Twiss and Unruh, 1998). For non-Andersonian type of cases, i.e. none of the paleostress orientations are vertical. Delvaux et al. (1997) suggested another numeric index (Φ') calculated from (Φ),where Φ' ranges from 0 to 3, as; $\Phi' = \Phi$ where σ1 close to vertical, $\Phi' = 2-\Phi$ where σ2 close to vertical and $\Phi' = 2 + \Phi$ where σ3 close to vertical. They also suggested Φ' values for different tectonic settings as; radial extensional ($0 < \Phi' < 0.25$), pure extensional ($0.25 < \Phi' < 0.75$), trans-tensional ($0.75 < \Phi' < 1.25$), pure strike-slip ($1.25 < \Phi' < 1.75$), trans-pressive ($1.75 < \Phi' < 2.25$), pure compressional ($2.25 < \Phi' < 2.75$) and radial compressional ($2.75 < \Phi' < 3$).

In this study, T-TECTO 3.0 software, using Gauss Method (Žalohar and Vrabec, 2007) is used for processing the fault kinematic data collected in the field such as fault plane attitudes and rake of slip lines because of its effectiveness on separating deformation phases in heterogeneous fields. The calculation process of the method mainly requires pre-defined values of three parameters, these are; (i) Parameter (s): Dispersion parameter of the distribution of angular misfits between the actual and resolved direction of slip along the fault. In the study,

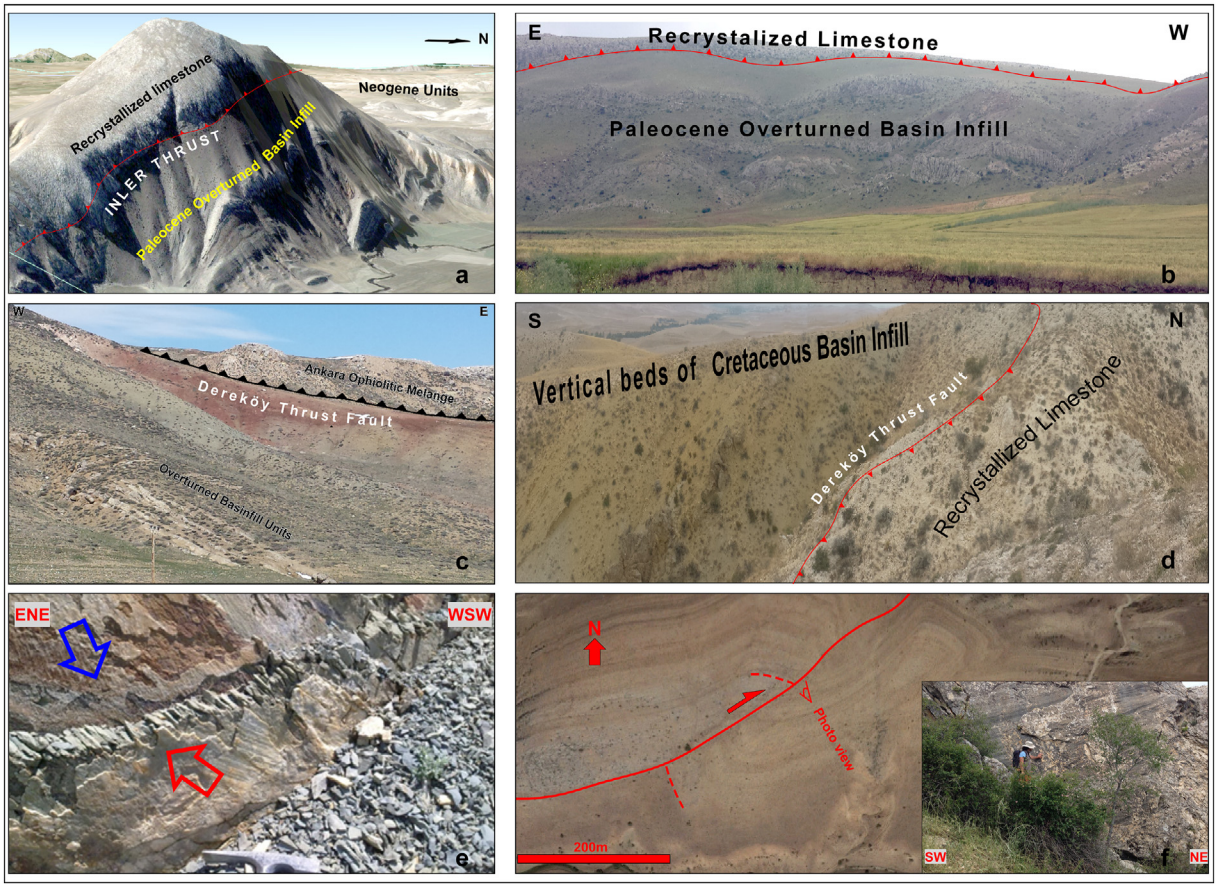

Fig. 4. (A) Google Earth image showing fault contact between basin infill and platform sequences along the İnler reverse fault. Location: East of İnler village. Note 3× vertical exaggeration in the image; (B) a view of İnler reverse fault and affected units (Zone 36, 437813 E, 4346138 N); (C) a view of Dereköy thrust fault and affected units (Zone 36, 462787 E, 4373255 N); (D) a view of Dereköy thrust fault and affected units (Zone 36, 455253 E, 4381645 N); (E) Overprinting slickensides observed in the deformation zone of the Dereköy thrust fault. View: towards NNW. Note that first movement (blue arrow) is normal indicated by striations, the second movement (red arrow) is reverse as indicated by calcite fibers (Zone 36, 459454 E, 4375790 N); (F) An example for a Neogene strike-slip fault, two dimensional view of a GoogleEarth image and close up view to the fault plane showing offset in the Çaldağ formation (Zone 36, 453498 E, 4361442 N). (For interpretation of the references to colour in this figure legend, the reader is referred to the web version of this article.)

parameter (s) were chosen as 20° in order to keep the possible irrelevant data out of the calculations, (ii) Parameter (d): Represent a threshold value for compatibility measure calculated by considering both misfit angle between actual and predicted direction of movement on the fault, and the position fault slip datum on Mohr diagram (the ratio of normal and shear stress on fault plane). The range for that parameter is suggested as > 60° for highly heterogeneous stress field and > 30° for less inhomogeneous stress fields by Žalohar and Vrabec (2007). In the study, this parameter was assigned as 45° due to the high possibility of having moderately heterogeneous stress filed in the sites, (iii) Parameter q1 and q2: (q1) defines the maximum residual frictional angle for activating pre-existing fractures whereas (q2) represents the angle of internal friction angle of an intact rock which will be fractured. In the study, (q1) and (q2) was assigned as 60° and 20° to take into account the possible re-activated fractures or the intact rocks having different internal friction angles.

Although fault plane attitudes and rake of slip lines are the main requirements of paleostress analyses, during data collection processes, displacement of the units, slip senses, and overprinting or cross-cutting relationships are also noted to differentiate deformation phases. After this separation, the data from individual sites are processed by considering the restrictions (parameters) mentioned above. After processing each site, if there are any residual measurements, they are re-processed, if the residual data satisfies the requirements of the processes. Otherwise they are deleted.

424 fault-slip measurements from 51 localities are collected under the context of kinematic studies. From these sites, 53 paleostress analyses are conducted and based on (Φ') index, two radial extensional, six pure extensional, five trans-tensional, nine strike-slip, fifteen trans-pressive, twelve pure compressional, and three radial pressive stress orientations are interpreted. However thirteen were determined to be spurious since they were incompatible with "*average pitch misfit angle versus number of faults*" diagram given in Orife and Lisle (2006). These unreliable results together with the reliable ones are summarized in Table 1 and Fig. 6, and cyclographic traces, slickensides and constructed paleostress configurations of the fault plane measurements are given in Appendix A.

3.2. Apatite (U-Th)/He dating

The main idea behind apatite-helium (AHe) dating technique relies on the ratio between the decay of uranium and thorium, and the amount of helium product (U-Th/He). Ages calculated by this method are generally younger than formation or sedimentation ages. The reason for getting younger ages is explained by the loss of helium products during cooling in the temperatures higher than closure temperature (Tc) of helium in apatite. Tc of the apatite-helium system was calculated ~68 ± 5 °C based on step wise heating diffusion experiments (Farley, 2000). In this regard, the ages determined in this study only represent the cooling/uplift duration of the samples below ~68 ± 5 °C.

Rock samples were collected only from detrital units spanning from

Table 1
Locations and the results of paleostress analyses (see Fig. 6A for locations).

Site	Longitude	Latitude	σ1	σ2	σ3	Φ	Φ′	n	Average pitch misfit angle°	Reliability*	Formation/cycle	Deformation phase
HY1	32.58519	39.39156	266/31	163/21	055/52	0.7	2.7	7	9	R	Kırkkavak/3	2
HY2	32.60343	39.41228	348/65	188/24	095/08	0.4	0.4	8	11	R	Kırkkavak/3	2
HY3	32.60587	39.41369	131/23	272/61	034/17	0.4	1.6	7	9	R	Yeşilyurt/2	1
HY4	32.61143	39.41863	088/02	357/36	181/54	0.2	2.2	7	7	R	Haymana/1	2
HY5	32.61317	39.42111	113/02	022/24	207/66	0.1	2.1	6	12	R	Haymana/1	2
HY6	32.56972	39.47018	072/12	309/68	166/18	0.1	1.9	6	17	R	Çayraz/4	2
HY7	32.53521	39.43755	015/02	105/02	240/87	0.3	2.3	10	16	R	J.Carbonates	2
HY8	32.51289	39.54457	351/13	084/12	215/73	0.3	2.3	7	6	R	Çaldağ/2	2
HY9	32.51173	39.54109	052/02	142/02	277/87	0.4	2.4	10	15	R	Yeşilyurt/2	2
HY10	32.35841	39.5787	196/23	056/61	293/17	0.3	1.7	5	6	R	Kartal/2	2
HY11	32.34941	39.57535	351/13	084/12	215/73	0.2	2.2	7	10	R	Kırkkavak/3	2
HY12	32.10503	39.44738	027/02	291/72	118/18	0.3	1.7	7	3	U	Kartal/2	2
HY13	32.10526	39.45166	351/13	084/12	215/73	0.1	2.1	6	5	R	Kartal/2	2
HY14	32.13187	39.44851	175/65	002/25	271/03	0.9	0.9	9	11	R	Kartal/2	2
HY15	32.13423	39.45285	236/02	326/02	101/87	0.8	2.8	7	3	U	Kırkkavak/3	2
HY16	32.13182	39.45945	309/13	214/23	065/63	0.6	2.6	8	4	U	ılgınlıkdere/3	2
HY17	32.17432	39.52801	098/34	309/52	198/15	0.9	1.1	7	5	R	E.polatlı/3	3
HY18	32.53072	39.48464	196/23	090/33	314/48	0.2	2.2	5	2	R	Çayraz/4	2
HY19	32.51121	39.48075	347/34	250/10	146/55	0.8	2.8	7	8	R	Ilgınlıkdere/3	2
HY20	32.52891	39.38742	019/23	118/22	247/57	0	2	7	24	U	E.polatlı/3	2
HY21	32.52964	39.38796	027/02	135/84	297/06	0.2	1.8	6	5	R	E.polatlı/3	2
HY22	32.31354	39.0945	346/02	080/60	255/30	0	2	11	7	U	Neogene	3
HY23A	32.51193	39.52666	046/65	232/25	141/03	0.5	0.5	7	9	R	Kartal/2	1
HY23B	32.51193	39.52666	115/23	021/11	267/64	0.4	2.4	10	9	R	Kartal/2	2
HY24A	32.56693	39.50942	030/13	298/12	166/73	0.5	2.5	18	22	R	Haymana/1	2
HY24B	32.56693	39.50942	094/55	322/26	220/23	0.6	0.6	5	7	R	Haymana/1	1
HY25	32.49576	39.42484	196/23	001/66	104/06	0.1	1.9	13	16	R	Haymana/1	2
HY26	32.50717	39.53027	327/34	059/02	151/56	0.5	2.5	13	15	R	Kırkkavak/3	2
HY27	32.11907	39.189	226/76	351/08	083/12	0.3	0.3	8	8	R	Neogene	3
HY28	32.55808	39.47286	045/65	245/24	152/08	1	1	6	2	U	Neogene	3
HY29	32.53761	39.48336	003/34	241/38	119/34	0	2	10	5	U	Çayraz/4	2
HY30	32.47419	39.44008	260/23	161/22	032/57	0.7	2.7	9	10	R	Haymana/1	2
HY31	32.37788	39.38725	002/86	271/00	180/04	0.4	0.4	9	10	R	Kırkkavak/3	2
HY32	32.37644	39.39714	035/23	254/61	132/17	0.6	1.4	9	10	R	ılgınlıkdere/3	2
HY33	32.26222	39.39058	348/65	201/21	106/12	0.4	0.4	6	9	R	Kırkkavak/3	2
HY34	32.20064	39.47947	162/02	252/12	063/78	0.2	2.2	10	16	R	Kırkkavak/3	2
HY35	32.08536	39.469	099/23	239/61	002/17	0.7	1.3	8	10	R	Kırkkavak/3	2
HY36	32.07489	39.44928	180/23	280/22	049/57	0.7	2.7	8	12	R	Kırkkavak/3	2
HY37	32.4605	39.49251	357/23	262/11	149/64	0.1	2.1	4	1	U	Yeşilyurt/2	2
HY38	32.47553	39.39523	305/65	204/05	112/24	0.2	0.2	4	3	U	Neogene	3
HY39	32.48101	39.38454	002/23	143/61	265/17	0.4	1.6	5	5	R	Kırkkavak/3	2
HY40	32.482	39.38541	284/44	096/46	190/04	0.8	1.2	6	2	U	Yeşilyurt/2	1
HY41	32.44642	39.38607	213/34	101/29	340/42	0.6	2.6	5	7	R	ılgınlıkdere/3	2
HY42	32.45021	39.38538	262/65	025/14	120/20	0.2	0.2	8	9	R	Yeşilyurt/2	1
HY43	32.45224	39.39777	187/02	093/60	278/30	0.6	1.4	10	4	U	Çaldağ/2	2
HY44	32.48194	39.38493	039/02	306/60	130/30	0.1	1.9	6	5	R	Kırkkavak/3	2
HY45	32.38865	39.27005	184/13	091/12	319/73	0.6	2.6	5	7	R	Kırkkavak/3	2
HY46	32.31789	39.25719	187/02	090/72	277/18	0.1	1.9	25	21	R	J.Carbonates	2
HY47	32.31792	39.25849	255/13	133/12	001/73	0.8	1.2	7	2	U	Çayraz/4	2
HY48	32.25637	39.28368	175/65	063/13	329/23	0.4	0.4	6	8	R	Neogene	3
HY49	32.27339	39.26793	334/02	243/24	068/66	0.8	2.8	6	3	U	Yeşilyurt/2	2
HY50	32.32745	39.41481	125/02	234/84	035/06	0.3	1.7	10	3	U	Neogene	3
HY51	32.3592	39.42932	099/23	264/66	007/06	0.7	1.3	8	9	R	Neogene	3

Φ stress ratio, Φ′ Numeric index of Delvaux et al. (1997), n: number of samples, * R - reliable, U-unreliable based on Orife and Lisle (2006).

Paleocene to Middle Eocene (Fig. 2A & B). Although eleven samples were collected, only five yielded sufficient apatite for He dating. (U-Th)/He ages were determined at the Scottish Universities Environmental Research Centre (SUERC) following procedures in Foeken et al. (2006). Alpha corrections were calculated by 10.2.2012 version of Flojt software using the criteria of Ketcham et al. (2011) and Gautheron and Tassan-Got (2010). The shapes of the grains and their alpha corrections ratios (F_t) are given in Appendix B. During calculations two different methods were used for determining the age of an individual sample which is represented by more than one apatite grain. The first method is the arithmetic mean and the second one is pooling. The pooling ages are determined by the procedures described in Vermeesch (2008) (Table 2). Durango AHe ages (n = 3) analyzed in this study gave an average age of 29.5 ± 2.9Ma. This age proves the reliability of the measurements since the standard Durango grains have a median age of 31.9 Ma.

4. Discussions

4.1. Kinematics of the basin

The most important faults in the region are the Dereköy (DT), İnler (İT) and Tepeköy (TY) thrust faults. The youngest unit affected by these faults is the middle Eocene rocks while Neogene units seal these structures. This relationship constrains the latest activity of the faults as post-Middle Eocene and pre-Neogene.

Other major structural elements in the basin are the folds (Figs. 2B & 5A), development of which is related to approximately NNE-SWW directed shortening, perpendicular to the basin bounding thrust faults. Except for the folds developed along the Yenimehmetli Fault Zone showing en echelon pattern implying sinistral motion, all other folds close to the margin of the basin or next to a thrust fault are almost

Table 2
Results of AHe age calculations (see Fig. 2B for sample locations).

Sample ID	238U (mol)	235U (mol)	232Th (mol)	4He (mol)	P(He mol/Ma)[b]	P (total)	He mol (total)	AHe age (Ma)	F_t[a]	AHe age (Ft corrected) (Ma)	Average AHe age (Ma)	Pooled AHe age (Ma)[c]
Th2-1	333.32	2.45	1533.29	33.24	0.89	3.42	92.33	37.4	0.855	43.8	32.70 ± 6.5	26.80 ± 2.6
Th2-2	102.37	0.75	511.01	8.06	0.28			28.3	0.803	35.3		
Th2-4	310.39	2.28	1794.47	19.72	0.93			21.1	0.862	24.5		
Th2-5	96.83	0.71	536.45	7.96	0.28			27.9	0.853	33.1		
Th2-6	266.37	1.96	2319.06	23.36	1.03			22.6	0.845	26.8		
Th3-1	144.33	1.06	1948.52	36.19	0.76	2.19	60.29	47.2	0.826	57.2	28.70 ± 14.5	29.18 ± 2.9
Th3-2	89.75	0.66	747.02	7.98	0.34			23.6	0.835	28.3		
Th3-4B	211.36	1.55	1037.61	6.59	0.58			11.3	0.802	14.1		
Th3-5	116.19	0.85	697.50	7.11	0.36			19.9	0.839	23.7		
Th3-6	55.14	0.41	259.06	2.42	0.15			16.3	0.806	20.2		
Th7-1	199.14	1.46	572.37	13.31	0.43	2.78	65.59	31.1	0.785	39.6	29.01 ± 5.9	23.56 ± 2.3
Th7-2	142.93	1.05	594.08	10.58	0.36			29.3	0.843	34.7		
Th7-3	149.28	1.10	963.33	9.84	0.48			20.5	0.848	24.2		
Th7-5	172.03	1.26	822.29	9.04	0.47			19.4	0.821	23.6		
Th7-6	169.93	1.25	446.29	8.53	0.35			24.2	0.817	29.6		
Th7-7	129.07	0.95	634.61	6.28	0.36			17.7	0.795	22.2		
Th7-9	124.57	0.91	594.50	8.00	0.34			23.7	0.812	29.2		
Th9-1	125.22	0.92	625.05	5.91	0.35	0.60	11.40	17.0	0.840	20.2	23.30 ± 3.1	17.77 ± 1.7
Th9-4	74.10	0.54	514.20	5.49	0.25			22.1	0.836	26.4		
Th11-2	39.25	0.29	572.57	2.50	0.22	2.18	38.58	11.3	0.774	14.7	26.16 ± 1.8	16.83 ± 1.7
Th11-3	64.48	0.47	336.22	1.61	0.18			8.8	0.800	11.0		
Th11-4	75.42	0.55	346.06	3.72	0.20			18.6	0.781	24.4		
Th11-5	347.13	2.55	899.65	6.20	0.72			8.7	0.792	10.9		
Th11-6	51.29	0.38	158.42	2.78	0.11			24.5	0.773	31.7		
Th11-8	105.55	0.78	220.99	5.31	0.20			26.3	0.750	35.0		
Th11-9	141.73	1.04	467.21	7.59	0.32			23.6	0.758	31.1		
Th11-10	48.32	0.35	558.95	8.86	0.23			38.7	0.766	50.5		
Du-4	1937.61	14.23	39,177.39	438.83	14.13	30.56	902.31	31.0		31.0 1	29.77 ± 1.1	29.46 ± 2.9
Du-5	1874.68	13.77	42,409.37	420.37	15.01			28.0		28.0		
Du-7	196.32	1.44	3935.12	43.12	1.42			30.3		30.3		

[a] Recoil correction, FT, based on of Ketcham et al. (2011) and Gautheron and Tassan-Got (2010), shapes of the grains are given in Appendix B.
[b] He production rate per million year, calculated based on decay constants of ^{238}U, ^{235}U and ^{232}Th and their total amounts in the grains.
[c] Calculated pooled ages, based on Vermeesch (2008), graphics of the calculations are given in Appendix C.

parallel. This implies that they are developed under the same deformation phase. In addition two major strike-slip faults, Yenimehmetli and Ataköy faults, are developed within the basin, which seems to displace the basin bounding thrust faults and cause structural segmentation of the basin. These structural segments are also marked by their different shortening ratios (Figs. 2B and 3) as very low (approx. %4) at the north and high (approx. %24) at the south. However the obtained 27° shortening amount is a local phenomenon that took place only within the Yenimehmetli Fault Zone and cannot be considered as a regional shortening for any part of the basin because the folds creating this amount of shortening are considered as en echelon products of the fault zone.

In addition to almost E-W directed thrust faults and folds (Fig. 5B & C). The strike-slip faults in the study area (Fig. 5D) are grouped as 1) NE-SW striking l strike-slip faults with chiefly sinistral component except for the Ataköy fault, 2) NW-SE striking right lateral strike-slip faults, 3) NE–SW striking both sinistral and dextral strike-slip faults.

In addition, paleostress inversion solutions and field observations indicate three phases of deformation in the region. These phases are defined by considering the possible relative ages of the measured fault planes and association of the paleostress inversion solutions that are explained by almost same paleostress configurations and almost same shape ratio index (Phi') of Delvaux et al. (1997) (Fig. 6 and Table 1). In this regard, (i) the first phase is characterized by measurements of normal fault planes that gave N-S extensional paleostress pattern (Fig. 4E), (ii) the second phase is characterize by thrust, normal and strike-slip fault plane measurements represented by almost N-S compressional and rarely E-W extensional paleostress solutions and (iii) the third phase is characterized by normal and strike-slip fault plane measurements showing NW-SE extension and or NW-SE compression possibly related to Neogene trans-current deformation of the basin since solution of this phase is represented by the faults cutting the Neogene units (Figs. 2B & 4F).

Integration of the kinematic data enables to construct an evolutionary structural model for the basin. This model indicates that (i) the study area was exposed to N-S extensional regime up to middle Paleocene, after that (ii) the main deformation events were related to almost N-S contraction causing pure-shear shortening in the basin up to Neogene (association of the structures developed under the contractional forces is explained in Fig. 5E by a left-lateral Riedel shear diagram developed under the effect of ~015°N-oriented maximum principal stress, σ1), and lastly (iii) the basin was exposed to Neotectonic trans-current regime. Association between the kinematic model and stratigraphy of the basin suggests that:

- The first phase corresponds to the deposition of first cycle units described as fore-arc sequences. This implies extensional fore-arc development probably due to the location of the trench and angle of the slab which allows extension (or thinning) perpendicular to the basin margins in the fore-arc region (Fig. 7A).
- Foreland deposition and fold and thrust belt development of the basin corresponds to the second phase.

4.2. Thermal history of the Basin

All samples are Lower Eocene to middle Paleocene sedimentary sequences of the Haymana Basin (Fig. 2A & B). By considering the temporal (stratigraphic) distribution of the samples, older AHe ages are expected for the samples of upper stratigraphic levels because they are thought to reach closure temperature (~70 °C) earlier than the lower level samples, during cooling processes. In the basin; this ideal AHe age distribution is not observed since Th9 and Th11 which are hosted by

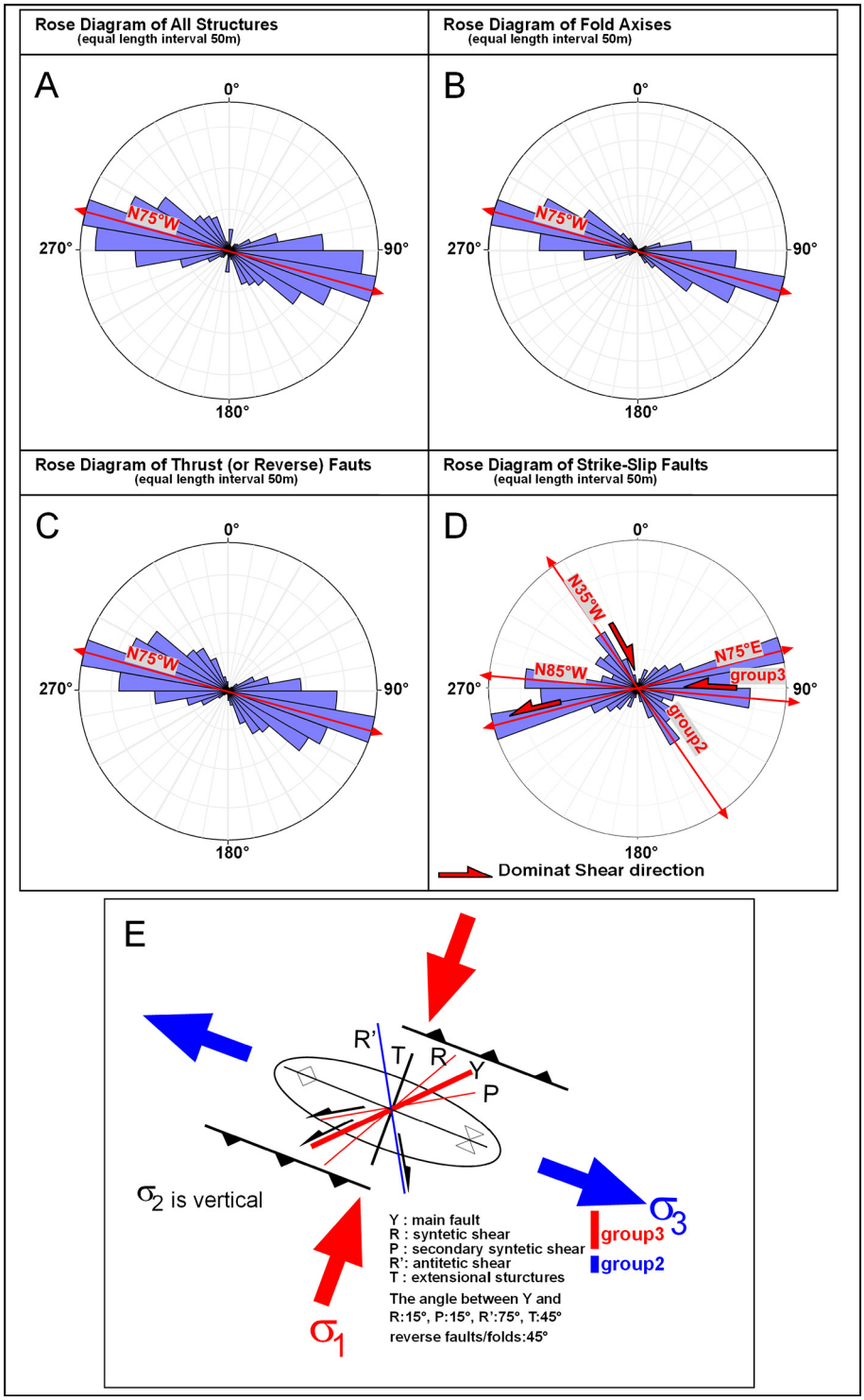

Fig. 5. (A) Length-weighted rose diagram of all structures of the Haymana Basin; (B) length-weighted rose diagram of folds of the Haymana Basin; (C) length-weighted rose diagram of thrust (or reverse) faults of the Haymana Basin; (D) length-weighted rose diagram of strike-slip faults of the Haymana Basin, see text for explanations; (E) left-lateral Riedel shear diagram developed by ~015°N oriented maximum principle stress direction (σ1), indicating possible trends of the structures in the Haymana Basin.

younger units yield youngest AHe ages (16.83 Ma and 17.77 Ma) (Fig. 2B). Therefore, the spatial distribution of the samples must also be taken into account. In this sense, the samples can spatio-temporally be grouped in two as the western group comprising Th9 and Th11, and the eastern group comprising samples Th3, Th2, and Th7 (Fig. 2B). In this case, an ideal AHe age distribution may be suggested for the eastern group because AHe ages get older towards upper stratigraphic levels. The same cannot be proposed for the western group, because AHe and stratigraphic ages of Th9 and Th11 are very close to each other. These groups are also separated by the Yenimehmetli fault zone. This fault is manifested by en echelon patterns of the folds in the field, and defines a boundary in the basin where shortening rates of the basin sharply decrease towards the north (Figs. 2B & 3).

The AHe ages indicate that the eastern part of the basin cooled due

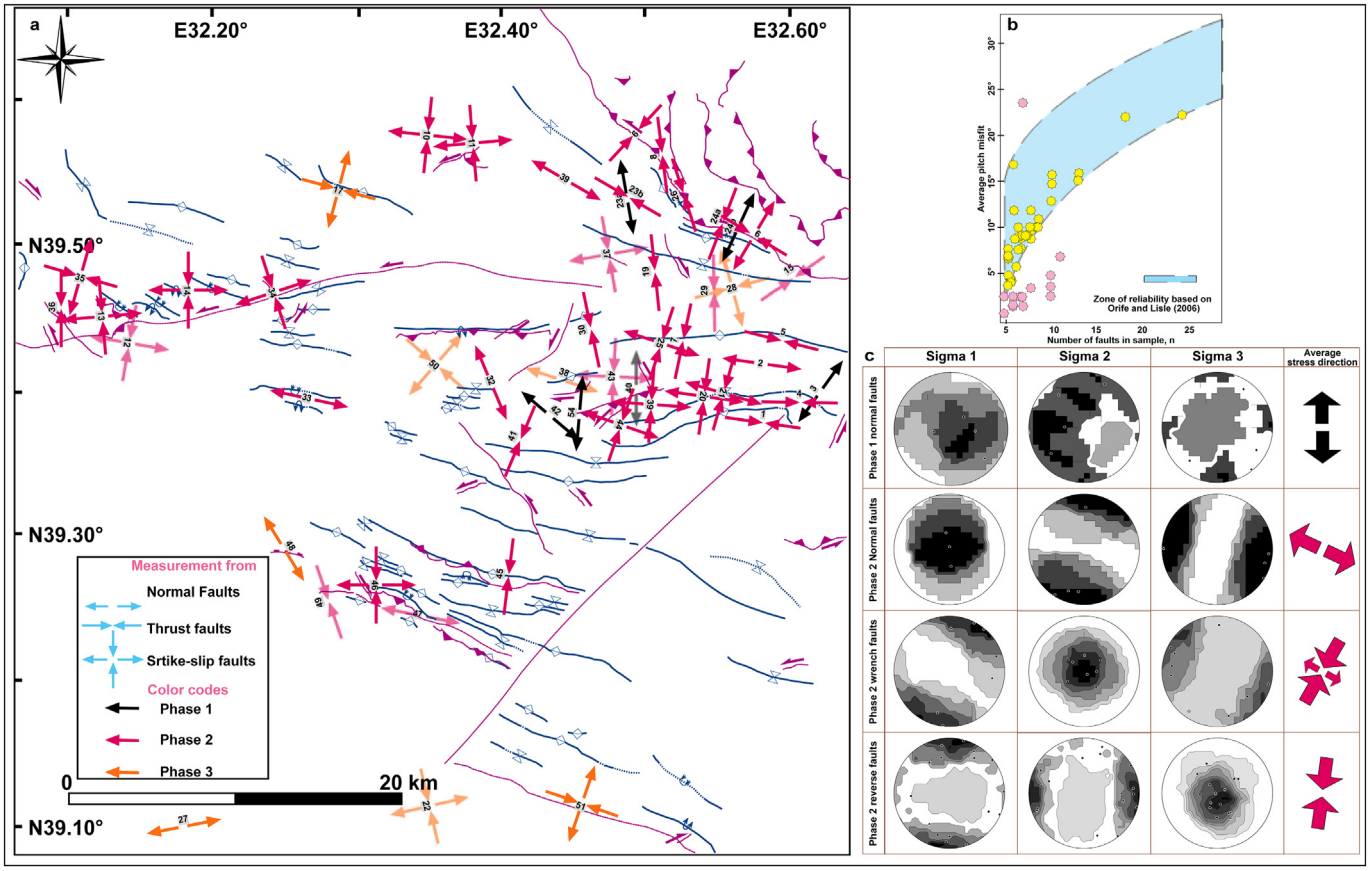

Fig. 6. (A) Major structures and paleostress orientations of deformation phases determined from all paleostress solutions including unreliable (shaded direction arrows) ones based on Orife and Lisle (2006); (B) Distribution of paleostress solutions on *average pitch misfit – number of fault in sample (n) diagram* showing reliable and unreliable solutions based on Orife and Lisle (2006); (C) Deformation phases (phase 1 and 2) based on paleostress inversion solutions. Contour diagrams of principle stress directions (sigma1-2-3) found after paleostress inversions. Each phase represents paleostress solutions coming from almost/probably same age (relatively dated) fault planes. Note that phases are represented by different type of faults and contour diagrams represent mean principle stress directions obtained from same types of faults. Each data point (black circles) represents principle stress direction of an individual paleostress inversion solution of a single paleostress location given in Table 1. Mean stress direction arrows represents a direction calculated from contour diagrams (stress direction of normal faults is the mean of sigma 3, stress direction of thrust/reverse faults is the mean of sigma 1, and stress direction of strike-slip faults with reverse component is the mean of sigma 1 and sigma 3. Arrows in "A" indicate stress directions found by paleostress inversion solutions and numbers on arrows are codes of paleostress measurement on Table 1.

to exhumation sometime before 29.18 Ma, whereas in the western part of the basin cooling started sometime later, ~17.77 Ma. This implies that the western part of the basin was exposed to contractional deformation for longer than the eastern parts. This might be explained by the progressive westward movement of the Derekoy fault which affected the western segment latterly. Movement of the fault is also supported in Özkaptan and Gülyüz (2019). Integration of AHe ages of the basin with the deformation phases indicates that Early Oligocene-Early Miocene time interval corresponds to fold and thrust belt development (phase 2) and the main uplift events in the region. This time interval also corresponds to the main vertical block rotations events of the basin (Özkaptan, 2016).

4.3. Regional implications

Although this study provides information mainly on post-Middle Eocene deformation of the region, some fault plane measurements from pre-Eocene units together with the stratigraphical background enable us to make inferences about the pre-Eocene fore-arc development of the basin. We suggest that late Cretaceous to Eocene evolution of the basin is in line with the evolution of the basins and crystalline rocks exposed along the central Pontides. Post-early Cretaceous geological development of the Central Pontides is represented by Turonian to Paleocene age arc-related intrusions and coeval volcano-sedimentary, back-arc, and fore-arc sequences but mainly with the Campanian ones (Koçyiğit, 1991; Tüysüz, 1999; Hippolyte et al., 2010, 2018). These rocks are defined as the last products of subduction along the İAESZ (Koçyiğit, 1991; Tüysüz et al., 1995; Koçyiğit, 1991; Rojay, 1991, 1995; Rojay and Süzen, 1997; Tüysüz, 1999; Kaymakci, 2000; Kaymakci et al., 2009). The Haymana basin is located at the southern tip of the Central Pontides and has only Pontide basement (Gülyüz, 2015). The tectonic position of the basin and our kinematic data together with the sedimentary background indicate almost N-S extension for this period suggests extensional fore-arc development on the Pontides as the other southern margin fore-arc basins such as Çankırı, Kırıkkale-Bala and Sivas basins (Fig. 7A). The presence of SSZ-type ophiolites (Önen, 2003; Çelik and Delaloye, 2006) and intra-oceanic subduction zone (Rojay, 2013; Hinsbergen et al., 2016) indicate a secondary subduction event in the south of the Haymana Basin might support evidence for the extension in the fore-arc region Although the reason for the extension in a such subduction setting might be driven various possibilities related to relative movement of the overriding and subducting plates, tectonic model proposed in Hinsbergen et al. (2016) indicating retreat of the subduction zone might simply explain the main reason behind the extension in fore-arc region.

Although the collision of the Pontides with the Tauride and Kırşehir blocks likely occurred in Paleocene to pre–early Miocene times (Koçyiğit et al., 1988; Koçyiğit, 1991; Rojay, 1995; Kaymakci, 2000;

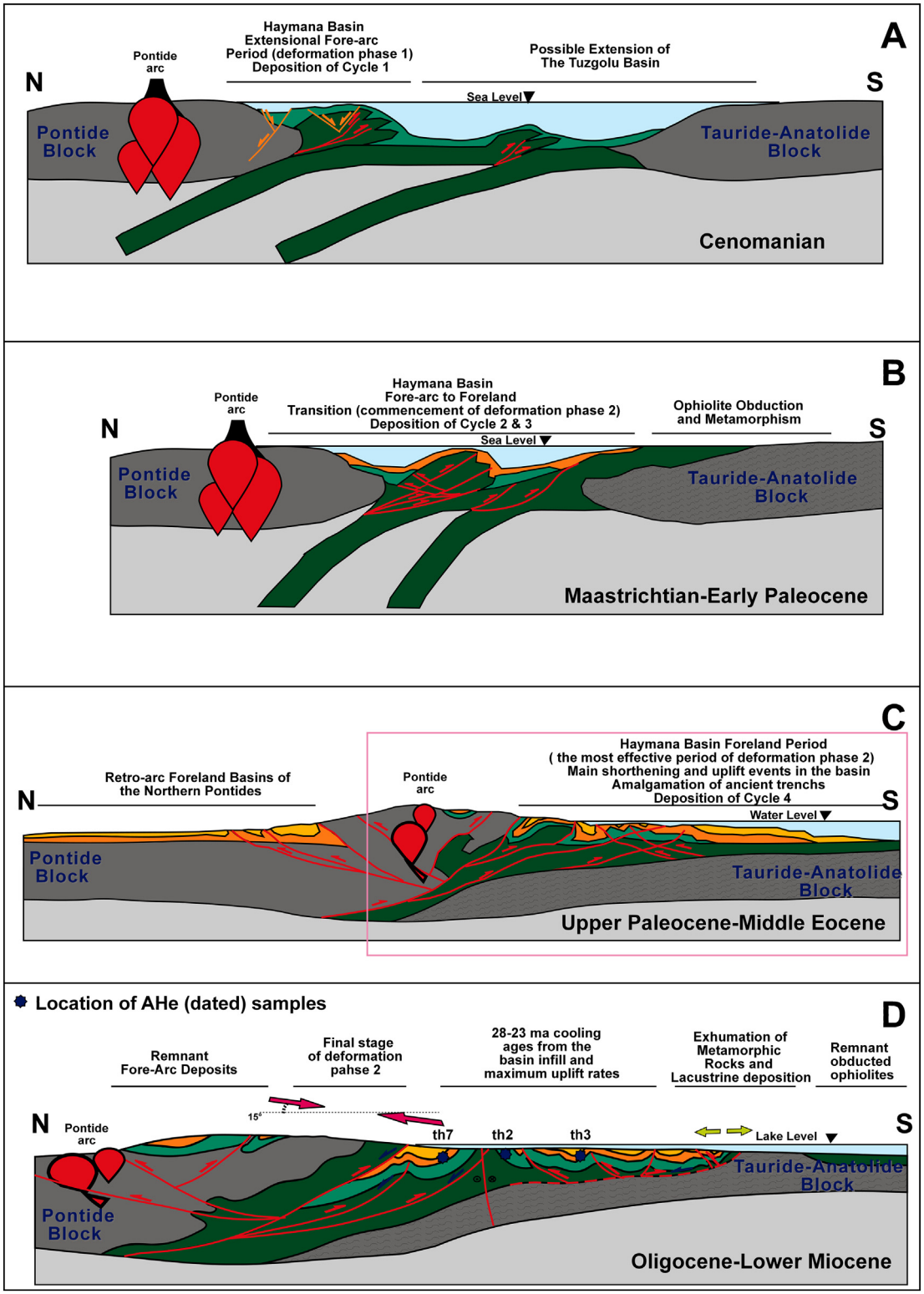

Fig. 7. A Conceptual model showing the tectonic evolution of the Haymana Basin with respect to Pontide and Tauride-Anatolide blocks during Late Cretaceous to Miocene time interval. (A) Cenomanian: extensional fore-arc development during deformation phase1, orange arrows indicate extensional faults in fore-arc region; (B) Maastrichtian- Early Paleocene: fore-arc to foreland transition, commencement of deformation phase2, ophiolite obduction and metamorphism of Tauride-Anatolide Block; (C) Upper Paleocene-Middle Eocene: foreland period of the basin, the most effective period of deformation phase2, amalgamation of ancient trenches, (D) Oligocene-Lower Miocene: Final stage of deformation phase2, exhumation of Tauride-Anatolide Block metamorphic rocks, structural segmentation of the basin along a strike slip (Yenimehmetli) fault. Note: (1) The presence of a southerly-located subduction zone is inferred from the studies of Önen (2003), and Çelik and Delaloye (2006) and Rojay (2013) and Hinsbergen et al. (2016), (2) Only possibly active faults are shown on each cartoon and the faults of the previous phases are not shown for the sake of simplicity, (3) Retro-arc foreland basins in "C" are inferred from Espurt et al. (2014), (4) Pink rectangle in "C" represents the coverage of "D", (5) Volcanic cones represent the active terms of the Pontide arc. Cartoons are not to the scale so the thicknesses of the units and blocks are not constant. (For interpretation of the references to colour in this figure legend, the reader is referred to the web version of this article.)

Kaymakci et al., 2009; Hippolyte et al., 2010; Özkaptan and Gülyüz, 2019), the timing of the collision of Pontides and Taurides around the Haymana region and timing of foreland and thrust belt development in front of the central Pontides is under debate. A post–early Paleocene age can, however, be inferred as the initiation age of the collision; the youngest peak metamorphic age (Pourteau et al., 2010, 2013, 2016, 2019) from the Afyon zone of Tauride Platform predating the collision event in the region. This is represented by compressional setting-related structures and retro-arc foreland or collisional-setting related deposition in the northern and southern Central Pontides, respectively (Koçyiğit et al., 1988; Koçyiğit, 1991; Rojay, 1991, 1995; Tüysüz, 1999; Kaymakci, 2000; Kaymakci et al., 2009; Hippolyte et al., 2010; Espurt et al., 2014). It may therefore be suggested that post–Early Paleocene evolution of the Haymana basin can be correlated with all of the central Pontide basins. In this sense, it is proposed that the deformation phase 2, that indicate N–S directed compression and related fold and thrust belt development in the Haymana Basin is attributed to this collisional period (Fig. 7B–D). Additionally, the apatite He ages presented in this study suggest that the effects of the collision lasted at least in early Miocene in the Haymana region.

5. Conclusions

1. The Haymana Basin is segmented into three parts as a northern segment, southern segment and southeastern segments. The boundaries between these segments are defined by strike-slip faults, namely Yenimehmetli and Ataköy faults.

- The northwestern segment is represented by NW–SE-trending folds and reverse/thrust faults which resulted in 3 to %5 shortening of the basin.
- The second segment is represented by dominantly E–W-trending folds and reverse/thrust faults which resulted in ~25% shortening ratios of the basin.

2. Approximately, 015°N oriented σ1 and vertical σ3 gave way to the development of E–W- to WNW–ESE-oriented folds, reverse/thrusts faults, and NNW–SSE-oriented right-lateral and NE–SW- to ENE–WSW-oriented left lateral strike-slip faults in the basin.
3. Paleostress inversion studies indicate that the Haymana Basin experienced three phase of deformation which was active during pre–middle Paleocene, middle Paleocene to middle Miocene and post–middle Miocene time intervals, respectively. The first phase is characterized by extensional deformation with sub-vertical σ1 and approximately N–S-oriented sub-horizontal σ3. The second phase is characterized by a complex stress pattern during which reverse, normal and strike-slip faults with reverse components developed in different parts of the study area. The third phase represents the Neogene deformation of the basin and is characterized by extensional and transcurrent tectonics in places.
4. The Haymana Basin was developed on the southernmost tip of the Central Pontides and comprises two distinct episodes of tectonic development: (1) fore-arc basin phase: the Haymana Basin was developed on the Pontides and accretionary wedge of the Northern Neo-Tethys Ocean during Late Cretaceous to middle Paleocene time interval; (2) foreland basin phase is related to the progressive collision of the Pontides during middle Paleocene to Oligocene time interval.
5. The collision between the Pontides and the Tauride Platform and post-collisional convergence period in the region are the main factors for the uplift and exhumation of the Haymana Basin during the post–middle Eocene to middle Miocene time interval.

Supplementary data to this article can be found online at https://doi.org/10.1016/j.tecto.2019.06.020.

Acknowledgements

This work is a part of the PhD study of Erhan Gülyüz and supported by the ÖYP Program of Turkish Government and partly by Darius Program coordinated by Eric Barrier in UPMC-Paris.

References

Advokaat, E.L., van Hinsbergen, D.D.J., Kaymakci, N., Vissers, R.L.M., Hendriks, B.W.H., 2014. Late Cretaceous extension and Palaeogene rotation related contraction in Central Anatolia recorded in the Ayhan-Büyükkışla basin. Int. Geol. Rev. 56, 1813–1836.
Anderson, E.M., 1951. The Dynamics of Faulting and Dyke formation with Application to Brittan. Oliver and Boyd, Edinburgh.
Angelier, J., 1979. Determination of mean principal direction of stress for a given fault population. Tectonophysics 56, 17–26.
Angelier, J., 1984. Tectonic analysis of fault slip data sets. J. Geophys. Res. 89, 5835–5848.
Angelier, J., 1994. Fault slip analysis and paleostress reconstruction. In: Hancock, P.L. (Ed.), Continental deformation. Pergamon Press, Oxford, pp. 53–101.
Armijo, R., Carey, E., Cisternas, A., 1982. The inverse problem in microtectonics and the separation of tectonic phases. Tectonophysics 82, 145–160.
Arslan, M., Temizel, İ., Abdioğlu, E., Kolaylı, H., Yücel, C., Boztuğ, D., Şen, C., 2013. ^{40}Ar–^{39}Ar dating, whole-rock and Sr–Nd–Pb isotope geochemistry of post-collisional Eocene volcanic rocks in the southern part of the Eastern Pontides (NE Turkey): implications for magma evolution in extension-induced origin. Contributions to Mineralogy and Petrography 166, 113–142.
Bott, M.P.H., 1959. The mechanics of oblique-slip faulting. Geol. Mag. 96, 109–117.
Boztuğ, D., Jonckheere, R.C., 2007. Apatite fission-track data from central-Anatolian granitoids (Turkey): constraints on Neo-Tethyan closure: Tectonics 26, TC3011.
Boztuğ, D., Jonckheere, R., Wagner, G.A., Yeğingil, Z., 2004. Slow Senonian and fast Paleocene–early Eocene uplift of the granitoids in the Central Eastern Pontides, Turkey: apatite fission-track results. Tectonophysics 382, 213–228.
Cavazza, C., Federici, I., Okay, A.I., Zattin, M., 2012. Apatite fission-track thermochronology of the Western Pontides (NW Turkey). Geol. Mag. 149, 133–140.
Çelik, Ö.F., Delaloye, M., 2006. Characteristics of ophiolite-related metamorphic rocks in the Beyşehir ophiolitic mélange (Central Taurides, Turkey), deduced from whole rock and mineral chemistry. J. Asian Earth Sci. 26, 461–476.
Çetin, H., Demirel, I.H., Gökçen, S.L., 1986. Haymana'nin (SW Ankara) dogusu ve batisindaki Üst Kretase-Alt Tersiyer istifinin sedimantolojik ve sedimanter petrolojik incelemesi. TJK Bülteni 29 (2), 21–33.
Çemen, İ., Göncüoğlu, M.C., Dirik, K., 1999. Structural evolution of the Tuzgölü Basin in Central Anatolia, Turkey. J. Geol. 107, 693–706.
Clark, M., Robertson, A., 2002. The role of the Early Tertiary Ulukışla Basin, southern Turkey, in suturing of the Mesozoic Tethys Ocean. J. Geol. Soc. 159 (6), 673–690.
Dahlstrom, C.D.A., 1969. Balanced cross-sections. Can. J. Earth Sci. 6, 743–757.
Darin, M., Umhoefer, P., Thomson, S., 2018. Rapid Late Eocene exhumation of the Sivas Basin (Central Anatolia) driven by initial Arabia-Eurasia collision. Tectonics. https://doi.org/10.1029/2017TC004954.
Delvaux, D., Moeys, R., Stapel, G., Petit, C., Levi, K., Miroshenko, A., Ruzhıch, V., Sankov, V., 1997. Paleostress reconstructions and geodynamics of the Baikal region, Central Asia, part 2. Cenozoic rifting. Tectonophysics 282, 1–38.
Espurt, N., Hippolyte, J.-C., Kaymakci, J.C.N., Sangu, E., 2014. Lithospheric structural control on inversion of the southern margin of the Black Sea Basin, Central Pontides, Turkey. Lithosphere 6, 26–34.
Farley, K.A., 2000. Helium diffusion from apatite: general behavior as illustrated by Durango fluorapatite. J. Geophys. Res. 105, 2903–2914.
Fayon, A.K., Whitney, D.L., Teyssier, C., Garver, J.I., Dilek, Y., 2001. Effects of plate convergence obliquity on timing and mechanisms of exhumation of a mid-crustal terrain, the Central Anatolian Crystalline Complex. Earth Planet. Sci. Lett. 192, 191–205.
Foeken, J.P.T., Stuart, F.M., Dobson, K.J., Persano, C., Vilbert, D., 2006. A diode laser system for heating minerals for (U-Th)/He chronometry. Geochem. Geophys. Geosyst. 7 (4), Q04015. https://doi.org/10.1029/2005GC001190.
Gautier, P., Bozkurt, E., Hallot, E., Dirik, K., 2002. Dating the exhumation of a metamorphic dome: geological evidence for pre-Eocene unroofing of the Nigde Massif (Central Anatolia, Turkey). Geol. Mag. 139 (5), 559–576.
Gautier, P., Bozkurt, E., Bosse, V., Hallot, E., Dirik, K., 2008. Coeval extensional shearing and lateral underflow during Late Cretaceous core complex development in the Nigde Massif, Central Anatolia, Turkey. Tectonics 27, TC1003.
Gautheron, C., Tassan-Got, L., 2010. A Monte Carlo approach to diffusion applied to noble gas/helium thermochronology. Chem. Geol. 273, 212–224.
Görür, N., Oktay, F.Y., Seymen, I., Şengör, A.M.C., 1984. Palaeotectonic evolution of the Tuzgölü basin complex. Central Turkey: sedimentary record of a Neo-Tethyan closure: Journal of the Geological Society of London Special Publications, v. 17 (1), 467–482.
Görür, N., Tüysüz, O., Şengör, A.M.C., 1998. Tectonic evolution of the central Anatolian Basins. Int. Geol. Rev. 40, 831–850.
Gülyüz, E., 2015. Tectono-stratigraphic and Thermal Evolution of the Haymana Basin, Central Anatolia, Turkey [Ph.D. Thesis]. Middle East Technical University, Turkey, pp. 200.
Gülyüz, E., Kaymakci, N., Meijers, M.J.M., van Hinsbergen, D.J.J., Lefebvre, C.J.C., Vissers, R.L.M., Hendriks, B.W.H., Peynircioğlu, A.A., 2013. Late Eocene evolution of

the Çiçekdağı Basin (central Turkey): syn-sedimentary compression during micro-continent–continent collision in central Anatolia. Tectonophysics 602, 286–299.
Hardcastle, K.C., 1989. Possible paleostress tensor configurations derived from fault- slip data in eastern Vermont and western New Hampshire. Tectonics 8, 265–284.
Hartz, E.H., Andresen, A., 1997. From collision to collapse: complex strain permutations in the hinterland of the Scandinavian Caledonides. Journal of Geophysical Research: Solid Earth 102 (B11), 24697–24711.
Hinsbergen, D., Maffione, M., Plunder, A., Kaymakci, N., Ganerød, M., Hendriks, B., Corfu, F., Gürer, D., de Gelder, G., Peters, K., McPhee, P., Brouwer, F., Advokaat, E., Vissers, R., 2016. Tectonic evolution and paleogeography of the Kırşehir Block and the Central Anatolian Ophiolites, Turkey. Tectonics. 35. https://doi.org/10.1002/2015TC004018.
Hippolyte, J.-C., Müller, C., Kaymakci, N., Sangu, E., 2010. Nannoplankton dating in the Black Sea inverted margin of Central Pontides (Turkey) reveals two episodes of rifting. In: Sosson, M., Kaymakci, N., Stephenson, R.A., Starostenko, V., Bergerat, F. (Eds.), Sedimentary Basin Tectonics From the Black Sea and Caucasus to the Arabian Platform: Geological Society of London. vol. 340. pp. 13–136.
Hippolyte, J.-C., Müller, C., Sangu, E., Kaymakci, N., 2018. Stratigraphic comparisons along the Pontides (Turkey) based on new nannoplankton age determinations in the Eastern Pontides: geodynamic implications. In: Sosson, M., Stephenson, R. a., Adamia, S. A. (eds), Tectonic Evolution of the Eastern Black Sea and Caucasus. Geol. Soc. Lond., Spec. Publ. 428, 323–358.
Homberg, C., Bergerat, F., Philippe, Y., Lacombe, O., Angelier, J., 2002. Structural inheritance and cenozoic stress fields in the Jura fold-and-thrust belt (France). Tectonophysics 357 (1–4), 137–158.
Hu, J.C., Angelier, J., 2004. Stress permutations: three-dimensional distinct element analysis accounts for a common phenomenon in brittle tectonics. Journal of Geophysical Research: Solid Earth 109 (B9).
Kaymakci, N., 2000. Tectono-stratigraphical evolution of the Cankiri Basin (Central Anatolia, Turkey) [Ph.D. thesis]: Geologica Ultraiectina, 247 p. Utrecht University. In: The Netherlands.
Kaymakci, N., Özçelik, Y., White, S.H., Van Dijk, P.M., 2009. Tectono-stratigraphy of the Çankiri Basin: late Cretaceous to early Miocene evolution of the Neotethyan suture zone in Turkey: Journal of the Geological Society of London Special Publications 311, 67–106.
Keskin, M., Genç, S.C., Tüysüz, O., 2008. Petrology and geochemistry of post-collisional Middle Eocene volcanic units in North-Central Turkey: evidence for magma generation by slab breakoff following the closure of the Northern Neotethys Ocean. Lithos 104, 267–305.
Ketcham, R.A., Gautheron, C., Tassan-Got, L., 2011. Accounting for long alpha-particle stopping distances in (U-Th-Sm)/He geochronology. Refinement of the baseline case. Geochim. Cosmochim. Acta 75, 7779–7791.
Koçyiğit, A., 1991. An example of an accretionary forearc basin from Central Anatolia and its implications for the history of subduction of Neo-Tethys in Turkey. Geol. Soc. Am. Bull. 103, 22–36.
Koçyiğit, A., Özkan, S., Rojay, B., 1988. Examples of the forearc basin remnants at the active margin of northern Neo-Tethys: development and emplacement ages of the Anatolian Nappe, Turkey: Middle East Technical University. J. Pure Appl. Sci. 3, 183–210.
Lacombe, O., 2012. Do fault slip data inversions actually yield “paleostresses” that can be compared with contemporary stresses? A critical discussion. Compt. Rendus Geosci. 44, 159–173.
Lacombe, O., Mouthereau, F., Kargar, S., Meyer, B., 2006. Late Cenozoic and modern stress fields in the western Fars (Iran): implications for the tectonic and kinematic evolution of central Zagros. Tectonics 25 (1). https://doi.org/10.1029/2005TC001831.
Lefebvre, C.J.C., 2011. The tectonics of the Central Anatolian crystalline complex: a structural, metamorphic and paleomagnetic study. In: UU Universiteit Utrecht (147 pag.). Departement Aardwetenschappen). PhD thesis, Utrecht.
Lefebvre, C., Peters, M., Kalijn, W., Philip, C., Brouwer, F.M., van Roermund, H.L.M., 2015. Thermal history and extensional exhumation of a high-temperature crystalline complex (Hirkadag Massif, Central Anatolia). Lithos 238, 156–173.
Legeay, E., Pichat, A., Kergaravat, C., Ribes, C., Callot, J.-P., Ringenbach, J.C., Bonnel, C., Hoareau, G., Poisson, A., Mohn, G., Crumeyrolle, P., Kavak, K., Temiz, H., 2018. Geology of the Central Sivas Basin (Turkey). Journal of Maps. https://doi.org/10.1080/17445647.2018.1514539.
Nairn, S.P., Robertson, A.H.F., Ünlügenç, U.C., İnan, N., Taslı, K., 2013. Tectonostratigraphic evolution of the Upper Cretaceous-Cenozoic central Anatolian basins: an integrated model of diachronous ocean basin closure and continental collision. Journal of the Geological Society of London Special Publication, v. 372, 343–384.
Okay, A.I., 1984. Distribution and characteristics of the northwest Turkish blueschists. Journal of the Geological Society of London Special Publications 17, 455–466.
Okay, A., Tüysüz, O., 1999. Tethyan sutures of northern Turkey. Geol. Soc. Spec. Publ. 156, 475–515.
Okay, A.I., Sunal, G., Sherlock, S., Altıner, D., Tüysüz, O., Kylander-Clark, A.R.C., Aygül, M., 2013. Early Cretaceous sedimentation and orogeny on the southern active margin of Eurasia: Central Pontides, Turkey. Tectonics 32, 1247–1271.
Okay, A., ALTINER, D., Kylander-Clark, A., 2019. Major Late Cretaceous mass flows in central Turkey recording the disruption of the Mesozoic Continental Margin. Tectonics. https://doi.org/10.1029/2018TC005076.
Önen, A.P., 2003. Neotethyan ophiolitic rocks of the Anatolides of NW Turkey and comparison with Tauride ophiolites. J. Geol. Soc. Lond. 60, 947–962.
Orife, T., Lisle, R.J., 2006. Assessing the statistical significance of palaeostress estimates: simulations using random fault-slips. J. Struct. Geol. 28, 952–956.
Özkaptan, M., 2016, Paleomagnetism of Central Anatolia, Turkey [Ph.D. thesis]: Middle East Technical University, Ankara, 210p.
Özkaptan, M., Gülyüz, E., 2019. Relationship between the anisotropy of magnetic susceptibility and development of the Haymana Anticline, Central Anatolia (Turkey). Turk. J. Earth Sci. 28, 103–121.
Özsayın, E., Dirik, K., 2007. Quaternary activity of Cihanbeyli Fault Zone (southern segment of Eskişehir-Sultanhanı Fault System), Central Anatolia, Türkiye. Turk. J. Earth Sci. 16, 471–492.
Pollard, D.D., Saltzer, S.D., Rubin, A.M., 1993. Stress inversion methods: are they based on faulty assumptions? J. Struct. Geol. 15 (8), 1045–1054.
Pourteau, A., Candan, O., Oberhänsli, R., 2010. High-pressure metasediments in central Turkey: constraints on the Neotethyan closure history: Tectonics, v. 29, TC5004.
Pourteau, A., Sudo, M., Candan, O., Lanari, P., Vidal, O., Oberhansli, R., 2013. Neotethys closure history of Anatolia: insights from ^{40}Ar–^{39}Ar geochronology and P–T estimation in high-pressure metasedimentary rocks. Journal of Metamorphic Geol. 31, 585–606.
Pourteau, A., Oberhänsli, R., Candan, O., Barrier, E., Vrielynck, B., 2016. Neotethyan closure history of western Anatolia: a geodynamic discussion. Int. J. Earth Sci. 105 (1), 203–224.
Pourteau, A., Scherer, E.E., Schorn, S., Bast, R., Schmidt, A., Ebert, L., 2019. Thermal evolution of an ancient subduction interface revealed by Lu–Hf garnet geochronology, Halilbağı Complex (Anatolia). Geosci. Front. https://doi.org/10.1016/j.gsf.2018.03.004.
Ramsay, J.G., 1967. Folding and Fracturing of Rocks, MacGraw Hill. N. Y. 1-568.
Riba, O., 1976. Syntectonic unconformities of the Alto Cardener, Spanish Pyrenees: a genetic interpretation. Sediment. Geol. 15 (3), 213–233.
Rice, S.P., Robertson, A.H.F., Ustaömer, T., 2006. Late Cretaceous-Early Cenozoic tectonic evolution of the Eurasian active margin in the Central and Eastern Pontides, northern Turkey. Journal of the Geological Society of London Special Publications 260, 413–445.
Rojay, B., 1991. Tectonostratigraphy and Neotectonic Characteristics of the Southern Margin of Merzifon-Suluova Basin (Central Pontides, Amasya) [Ph.D. thesis]. Middle East Technical University, Ankara, pp. 105.
Rojay, B., 1995. Post-Triassic evolution of Central Pontides: evidence from Amasya region. Northern Anatolia: Geologica Romana 31, 329–350.
Rojay, B., 2013. Tectonic evolution of the Cretaceous Ankara ophiolitic mélange during the Late Cretaceous to pre-Miocene interval in Central Anatolia. Turkey: Journal of Geodynamics 65, 6–81.
Rojay, B., Süzen, L., 1997. Tectonostratigraphic evolution of an arc-trench basin on accretionary ophiolitic mélange prism, central Anatolia. Turkey: Association of Turkish Petroleum Geologist Bulletin 9, 1–12.
Şengor, A.M.C., Yilmaz, Y., 1981. Tethyan evolution of Turkey - a plate Tectonic approach. Tectonophysics 75 (3–4), 181–241.
Shan, Y., Suen, H., Lin, G., 2003. Separation of polyphase fault/slip data: an objective function algorithm based on hard division. J. Struct. Geol. 25 (6), 829–840.
Sirel, E., 1975. Polatlı (GB Ankara) güneyinin stratigrafisi: TJK Bülteni 18 (/2), 181–192.
Sirel, E., 1976. Haymana (G Ankara) yöresi İlerdiyen. Küiziyen ve Lütesiyen'deki Nummulites, Assilina ve Alveolina cinslerinin bazı türlerinin tanımlamaları ve stratigrafik dağılımları: TJK Bülteni 19, 31–44.
Sirel, E., Dağer, Z., Sözeri, B., 1986. Some biostratigraphic and paleogeographic observations on the Cretaceous-Tertiary boundary in the Haymana-Polatlı region (Central Turkey): in Walliser O. (ed) Global Bioevents. Lect. Notes Earth Sci. 8, 385–396.
Speciale, P.A., Catlos, E.J., Yıldız, G.O., Shina, T.A., Black, K.N., 2014. Zircon ages from the Beypazarı granitoid pluton (north central Turkey): tectonic implications. Geodin. Acta 25 (3–4), 162–182.
Sperner, B., and Zweigel P., 2010, A plea for more caution in fault–slip analysis: Tectonophysics, v, 482, p. 29–41.
Toker, V., 1979. Haymana yöresi (GB Ankara) Üst Kretase planktonik foraminiferaları ve biyostratigrafi incelemesi. TJK Bülteni 22, 121–132.
Toprak, V., Savascı, Y., Güleç, N., Tankut, A., 1996. Structure of the Galetean Volcanic Province, Turkey. Int. Geol. Rev. 38, 747–758.
Tüysüz, O., 1999. Geology of the Cretaceous sedimentary basins of the Western Pontides. Geol. J. 34, 75–93.
Tüysüz, O., Dellaloğlu, A.A., Terzioğlu, N., 1995. A magmatic belt within the Neo-Tethyan suture zone and its role in the tectonic evolution of Northern Turkey. Tectonophysics 243, 173–191.
Twiss, R.J., Unruh, J.R., 1998. Analysis of fault slip inversions: do they constrain stress or strain rate? J. Geophys. Res. 103, 12205–12222.
Ünalan, G., Yüksel, V., Tekeli, T., Gönenç, O., Seyirt, Z., Hüseyin, S., 1976. Haymana-Polatlı yöresinin (Güneybatı Ankara) Üst Kretase-Alt Tersiyer stratigrafisi ve paleocoğrafik evrimi. TJK Bülteni 19, 159–176.
Vermeesch, P., 2008. Three new ways to calculate average (U-Th)/He ages. Chem. Geol. 249, 339–347.
Wallace, R.E., 1951. Geometry of shearing stress and relation to faulting. J. Geol. 69, 118–130.
Whitney, D.L., Teyssier, C., Dilek, Y., Fayon, A.K., 2001. Metamorphism of the Central Anatolian Crystalline Complex, Turkey: influence of orogen-normal collision vs wrench-dominated tectonics on P-T-t paths. J. Metamorph. Geol. 19, 411–432.
Whitney, D.L., Umhoefer, P.J., Teyssier, C., Fayon, A.K., 2008. Yo-yo tectonics of the Nigde Massif during wrenching in central Anatolia. Turk. J. Earth Sci. 17, 209–217.
Žalohar, J., Vrabec, M., 2007. Paleostress analysis of heterogeneous fault-slip data: the Gauss method. J. Struct. Geol. 29, 1798–1810.